small structures
www.small-structures.com

Power of the Many-Body Force: Magnitudes and Angles of Atomic Van der Waals Dispersion Forces in Extended Molecular Systems

*Raul Ian Sosa, Mario Galante, and Alexandre Tkatchenko**

A distinctive feature of soft materials such as polymers, liquids, biomolecules, and nanostructures is that their macroscopic properties are highly dependent on structural dynamics, even at equilibrium. This is a consequence of fewer covalent bonds when compared to hard solids, which grants soft materials higher structural flexibility, mostly controlled by noncovalent forces such as van der Waals dispersion (vdW) interactions. Although vdW energies have been investigated thoroughly in a wide range of systems, much less is known about the magnitudes and orientations of atomic vdW forces beyond the highly approximate pairwise (PW) Lennard–Jones-like potentials. The present study compares PW and quantum-mechanical many-body vdW forces in large molecular systems with a varying degree of structural order. Many-body effects can enhance atomic vdW forces by up to 300% and introduce significant angular deviations of up to 60 degrees on average. The changes in the power-law decay rate alone account for a significant portion of the many-body contributions, indicating that an effective PW potential tailored to reproduce the decay rate of many-body dispersion will already be more accurate than standard models. These results highlight how collective phenomena in soft matter can be rationalized through a more accurate quantum-informed perspective on vdW forces.

1. Introduction

Van der Waals (vdW) interactions play a critical role in complex molecular systems across diverse fields such as materials science, biology, and engineering.[1–4] These interactions, arising from quantum-mechanical electron density fluctuations, significantly influence phenomena ranging from protein interactions and folding to the self-assembly of nanostructures.[5–7] Accurately capturing vdW forces is essential for predicting dynamical behaviors—such as vibrations, mechanical responses, and diffusion processes—in materials like molecular crystals, polymers, and biological macromolecules.[8,9] These properties are governed by atomic vdW forces away from equilibrium, which dictate how atoms and molecules move and interact over time. Although much of the previous focus has been on accurately describing vdW energies for static configurations,[10,11] understanding and predicting dynamical phenomena require precise vdW force models. Energies predominantly provide information on the stability and equilibrium configurations of a given system, but it is the forces that directly drive the kinetics and pathways of dynamical processes such as failure mechanisms in materials and macroscale plasticity.[12–15]

Accurately describing vdW forces in large-scale systems remains computationally challenging.[16] Lennard–Jones (LJ) potentials and other pairwise (PW) models, while computationally efficient, fail to capture the full complexity of vdW interactions in realistic systems and fully reproduce experimental observations.[17–20] This limitation arises because PW approaches neglect screening and the many-body effects that emerge from the collective behavior of multiple interacting particles. More advanced methods, such as the many-body dispersion (MBD) approach, yields significantly improved accuracy, but come at higher computational cost.[21]

The MBD method[21–24] considers collective many-body interactions and screening effects over longer ranges. As illustrated in **Figure 1**(a), the MBD method models vdW interactions by treating atoms as quantum Drude oscillators (QDOs) that are coupled via dipole–dipole interactions. This approach inherently captures the many-body correlations and the spatial extension characteristic of vdW dispersion forces, thus yielding nonadditive force contributions that are crucial for accurate prediction of properties of soft materials. The inclusion of beyond PW vdW interactions has been shown to yield estimations that are in better agreement with experimental results for phenomena such as thin-layer delamination,[25] organic molecular materials,[19] and interlayer separation in 2D materials.[26]

R. I. Sosa, M. Galante, A. Tkatchenko
Department of Physics and Materials Science
University of Luxembourg
Luxembourg City L-1511, Luxembourg
E-mail: alexandre.tkatchenko@uni.lu

M. Galante
School of Molecular Sciences
Arizona State University
Tempe 85287, USA

The ORCID identification number(s) for the author(s) of this article can be found under https://doi.org/10.1002/sstr.202500226.

DOI: 10.1002/sstr.202500226

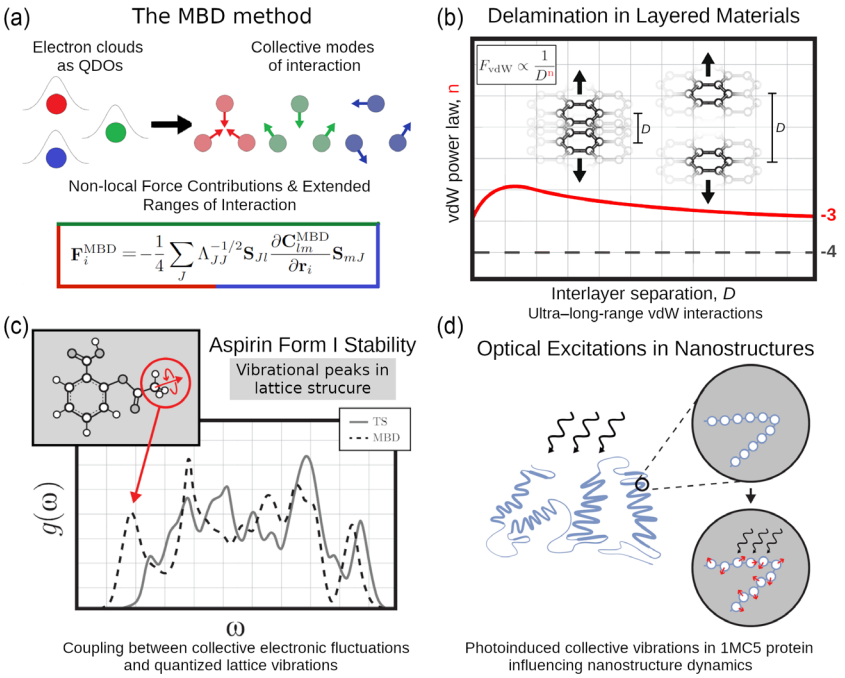

Figure 1. a) Schematic representation of the MBD method, in which valence electrons are approximated as QDOs that collectively interact through dipole–dipole coupling, generating collective electronic fluctuation modes. vdW energies are derived from these modes, and the resulting forces inherently include nonlocal contributions. b) Graphene delamination and vdW interaction decay denote that MBD predicts a slower decay of the vdW interaction than PW methods.[26] c) Phonon density of states in Aspirin form I schematic comparing both the TS PW method and the MBD method. Many-body effects shape the forces responsible for this polymorph's stability.[29] d) Optical excitations in nanostructures and protein systems, where MBD predicts collective vibrations in 1MC5 upon optical excitation, influencing nanostructure dynamics.[30]

Many interfacial phenomena in layered materials are governed by interactions at the micro and nanoscale, including adhesion and cohesion at interfaces.[27] In graphene delamination, MBD predicts a slower decay of vdW forces with increasing interlayer separation than PW methods, aligning with experimental observations of extended interaction ranges in layered materials, as shown in Figure 1(b).[26] This result implies significant interlayer forces even at larger separations, thus influencing the mechanical and adhesive properties of layered systems. Recent experimental atomic force microscopy studies in multilayer structures suggest that PW dispersion theories tend to overestimate substrate contributions at critical adhesive pressures.[28] By contrast, MBD accurately reproduces these observed interactions, indicating the importance of including many-body effects in vdW force calculations. Furthermore, the role of MBD in vibrational spectra has been examined in molecular crystals such as aspirin.[29] Figure 1(c) displays the phonon density of states in the form I of aspirin, where the coupling between collective electronic fluctuations and quantized lattice vibrations modifies the forces at play in stabilizing this specific polymorph. Including many-body vdW effects leads to improved predictions of vibrational modes, which is crucial for understanding the thermodynamic stability and response of crystalline materials. Finally, Figure 1(d) illustrates how MBD has also been applied to predict collective photoinduced vibrations in the 1MC5 protein.[30] The refined description of vdW forces influences the dynamics of the nanostructure, providing insights on processes such as energy transfer in biological systems.

Nevertheless, this increase in accuracy comes at a computational cost; the computational limitation of MBD is particularly problematic in large-scale molecular systems, such as polymer melts, biological macromolecules, and layered materials, which can consist of millions of atoms and exhibit a rich diversity of molecular structures and interactions.[31] In such systems, the need to balance computational efficiency with accuracy is paramount. To address this, we seek the development of methods that can retain the computational efficiency of PW models while incorporating essential features of many-body vdW interactions to capture long-range and global effects. By developing such methods, it becomes possible to accurately simulate large-scale systems and their dynamical behaviors governed by vdW forces without incurring prohibitive computational costs.

To achieve this goal, it is crucial to first understand how many-body effects influence vdW forces in various molecular systems. By thoroughly analyzing MBD force predictions and identifying patterns in their magnitudes, ranges, and orientations of force vectors, we can gain insights into the essential features of many-body interactions that need to be captured in simplified models. This understanding is vital for developing coarse-grained methods that effectively incorporate the key aspects of many-body vdW interactions while maintaining computational efficiency.

In this work, we perform a detailed analysis of many-body vdW forces across molecular systems ranging from small molecules to complex materials (see **Figure 2**). By systematically comparing the forces obtained from the computationally efficient

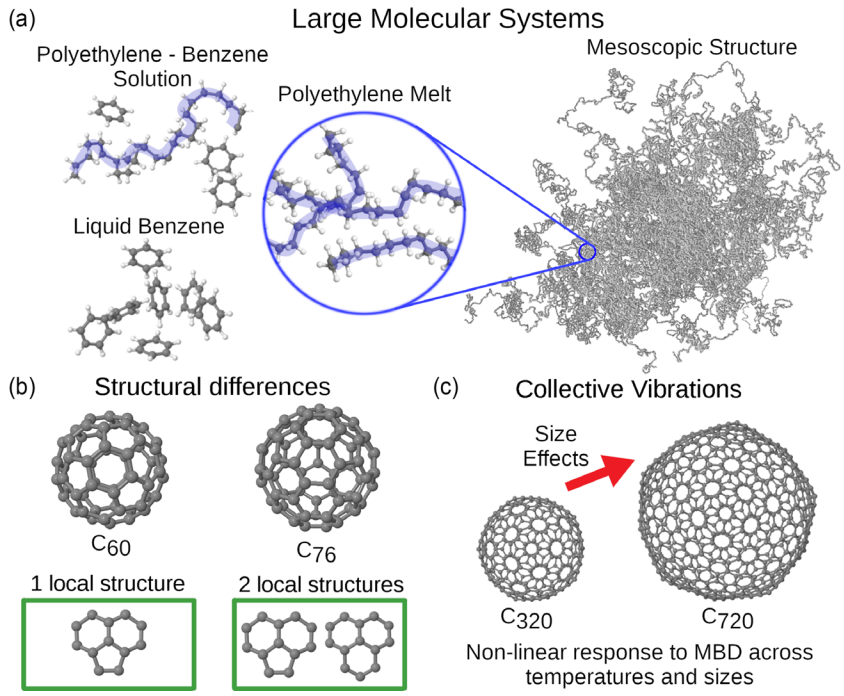

Figure 2. a) Top left: Depictions of the three large molecular systems—the polyethylene-benzene solution, benzene liquid, and polymer melt. These configurations are obtained using classical force fields at 300 K. Top right: Visualization of the entangled polyethylene melt, with a zoomed-in view highlighting the microscopically complex and disordered nature of the polyethylene chains (shown in blue). b) Structures of C_{60} and C_{76} fullerenes. C_{60} exhibits high symmetry with indistinguishable atomic environments, while C_{76} has lower symmetry with two distinct local atomic arrangements. c) Depictions of the C_{320} and C_{720} fullerenes. Size and temperature effects due to MBD were observed across the two benchmark systems.

PW Tkatchenko–Scheffler (TS) method[32] with those from the more accurate MBD method,[21] we uncover substantial differences in force magnitudes, ranges, and directions. Our study encompasses complex systems such as polymer melts, benzene solutions, and polyethylene dissolved in benzene (Figure 2(a)), as well as small molecules like fullerenes C_{60} and C_{76} (Figure 2(b)), and big molecules like fullerenes C_{320} and C_{720} (Figure 2(c)). The large molecular systems feature diverse local atomic environments, making them ideal for analyzing vdW interactions in realistic materials. The small fullerenes allow us to examine the role of molecular symmetry; C_{60} is highly symmetric with uniform atomic environments, whereas C_{76} has lower symmetry with multiple distinct local configurations. Long molecular dynamics simulations for C_{320} and C_{720} make it possible to identify size and temperature effects in the collective vibrations of these systems induced by MBD. Our analysis demonstrates that molecular topology and complexity significantly affect vdW force predictions, with larger discrepancies in less uniform systems as a result of pronounced many-body effects not captured by PW (or even three-body) models.

2. Methodology: PW versus Many-Body vdW Models

The TS method extends traditional empirical PW approaches by incorporating information about the local electronic environment through the scaling of atomic polarizabilities and dispersion coefficients based on Hirshfeld volume ratios.[32,33] This environment-dependent strategy uses the system's electron density partitioning to more accurately reflect the influence of nearby atoms on each site's effective polarizability. As a result, TS provides considerably improved predictions of vdW interactions over simpler LJ potentials in many molecular and condensed-phase systems, offering a balance between computational efficiency and a more physically grounded description of dispersion forces. This approach has been shown to perform well across various molecular databases, including recent large-scale benchmarks.[34] Despite these improvements, the TS method remains fundamentally PW and does not capture the nonadditive many-body effects arising from collective electronic fluctuations, which detracts from its comparison with experimental observations.[17,19,20] As a result, TS PW forces are always collinear with the vector connecting pairs of atoms. The vdW energy in the TS method is expressed as

$$E_{\mathrm{vdW}}^{\mathrm{TS}} = -\frac{1}{2}\sum_{i\neq j} f_{\mathrm{damp}}(r_{ij}, R_{ij}^{0})\frac{C_{6,ij}}{r_{ij}^{6}} \quad (1)$$

where r_{ij} is the distance between atoms i and j, $C_{6,ij}$ are the environment-dependent dispersion coefficients, R_{ij}^{0} is the sum of vdW radii, and f_{damp} is a Fermi-type damping function fitted to reproduce intermolecular interaction energies of benchmark databases.[22,32,35]

In contrast, the MBD method extends beyond PW interactions by treating atoms as QDOs coupled through long-range dipole–dipole interactions, as depicted in Figure 1(a).[21] This approach inherently captures many-body effects and the collective nature of vdW interactions. Consequently, MBD forces exhibit significant noncollinearity due to the coupling of collective electronic fluctuations, and they display altered decay behaviors compared to PW forces, with effective power-law exponents deviating from the classical r^{-6} decay typical of PW vdW interactions.[22]

The MBD method calculates the vdW energy by explicitly considering the collective electronic fluctuations in its energy expression

$$E_{\mathrm{vdW}}^{\mathrm{MBD}} = \frac{\hbar}{2}\sum_{p=1}^{3N}\widetilde{\omega}_p - \frac{3\hbar}{2}\sum_{i=1}^{N}\omega_i \tag{2}$$

where $\widetilde{\omega}_p$ are the collective plasmon-like eigenfrequencies obtained by diagonalizing the interaction matrix $\mathbf{C}^{\mathrm{MBD}}$, and ω_i are the characteristic frequencies of the individual atomic QDOs. This results in a many-body energy expression which, in contrast to the PW TS (Equation 1), has no explicit interaction decay rate between the constituent parts of the system.

The interaction matrix $\mathbf{C}^{\mathrm{MBD}}$ is composed of $N \times N$ blocks of size 3×3 that account for the coupling between each pair of atoms i and j (with Cartesian components a, b)

$$C_{\mathrm{ij}}^{\mathrm{MBD,ab}} = \omega_{\mathrm{i}}^2\delta_{\mathrm{ij}}\delta_{\mathrm{ab}} + (1-\delta_{\mathrm{ij}})\omega_{\mathrm{i}}\omega_{\mathrm{j}}\sqrt{\alpha_{\mathrm{i}}^0\,\alpha_{\mathrm{j}}^0}\,T_{\mathrm{ij,damped}}^{\mathrm{ab}} \tag{3}$$

where α_{i}^0 is the static dipole polarizability of atom i, and δ_{ij} is the Kronecker delta. The damped dipole–dipole interaction tensor, $T_{\mathrm{ij,damped}}^{\mathrm{ab}}$, incorporates a distance-dependent screening function $f_{\mathrm{damp}}(r_{ij};\beta)$

$$T_{\mathrm{ij,damped}}^{\mathrm{ab}} = f_{\mathrm{damp}}(r_{\mathrm{ij}};\beta)\left(\frac{3r_{\mathrm{ij}}^{\mathrm{a}}r_{\mathrm{ij}}^{\mathrm{b}}}{r_{\mathrm{ij}}^5} - \frac{\delta_{\mathrm{ab}}}{r_{\mathrm{ij}}^3}\right) \tag{4}$$

with the displacement vector $\mathbf{r}_{\mathrm{ij}} = \mathbf{r}_{\mathrm{i}} - \mathbf{r}_{\mathrm{j}}$ connecting atomic sites i and j, and $r_{\mathrm{ij}} = |\mathbf{r}_{\mathrm{ij}}|$. The function $f_{\mathrm{damp}}(r_{\mathrm{ij}};\beta)$ effectively reduces overestimated dipole–dipole interactions at short range, with β being the only empirically fitted parameter in the model as per the MBD@rsSCS scheme.[22]

Diagonalization of the interaction matrix yields the eigenvalues $(\widetilde{\omega}_p)^2$ and the transformation matrix $\mathbf{S}$

$$\mathbf{S}^{\mathrm{T}}\mathbf{C}^{\mathrm{MBD}}\mathbf{S} = \Lambda \tag{5}$$

where Λ is the diagonal matrix of squared collective frequencies $(\widetilde{\omega}_p)^2$.

By taking the gradient of the MBD energy with respect to atomic positions, we obtain the vdW forces

$$\mathbf{F}_i^{\mathrm{MBD}} = -\frac{\partial E_{\mathrm{vdW}}^{\mathrm{MBD}}}{\partial \mathbf{r}_i} = -\frac{1}{4}\sum_{\mathrm{J}}\Lambda_{\mathrm{JJ}}^{-1/2}\mathbf{S}_{\mathrm{Jl}}\frac{\partial \mathbf{C}_{\mathrm{lm}}^{\mathrm{MBD}}}{\partial \mathbf{r}_i}\mathbf{S}_{\mathrm{mJ}} \tag{6}$$

where the indices l, m run over atomic degrees of freedom (including Cartesian components), J runs over the collective modes, and repeated indices imply summation.

In this expression, $\Lambda_{\mathrm{JJ}} = (\widetilde{\omega}_{\mathrm{J}})^2$ are the eigenvalues from the diagonalization, $\mathbf{S}$ is the transformation matrix containing the eigenvectors, and $\frac{\partial \mathbf{C}_{\mathrm{lm}}^{\mathrm{MBD}}}{\partial \mathbf{r}_i}$ represents the derivative of the interaction matrix with respect to the position of atom i.

The electric response of each atom is represented by a quantum drude oscillator, and interatomic forces are the result of the dipole–dipole interactions between all QDOs. Therefore, their direction is determined by the competition between the $3N$ normal modes of charge oscillations, which in most cases deviates from the direction given by the interatomic distance vector, that is characteristic of PW approximations. We will refer to this misalignment between PW and MBD forces as the noncollinearity of the latter. We remark that this is a consequence of the collectivity of charge oscillations, meaning that altering the position, mass, or oscillator frequency of a single QDO can induce a change in the forces across the entire system.

The bottleneck of an MBD calculation lies in the diagonalization of the coupling matrix $\mathbf{C}^{\mathrm{MBD}}$ as shown in Equation 5, thus the computational cost of MBD scales as $O(N^3)$ with the number of atoms N. Dense diagonalization of this matrix ensures that all many-body correlations are accounted for in determining the final dispersion energy and forces. Although iterative or sparse approaches can sometimes alleviate the worst-case N^3 overhead in special contexts, the generic dense case remains $O(N^3)$ for standard eigenvalue calculations.[36,37] This scaling limitation emphasizes the importance of developing computational methods that preserve the essential features of MBD while being more tractable for simulations of large and complex systems.

While the PW TS model and the MBD method employed in this work belong to a recognized class of quantum mechanics-informed approximations with minimal empiricism, both approaches deliver reliable accuracy for finite molecules and periodic solids.[9,38] They effectively represent key screening effects and collective electronic behavior within a broad range of systems. In recent years, alternatives such as uMBD, designed for strongly ionic materials,[39] and MBD-NL, which unifies the modeling of molecules and materials,[40] have further expanded the capabilities of quantum-based dispersion methods. Even so, materials exhibiting nontrivial interactions between delocalized conduction electrons and localized states remain challenging,[41] indicating that further refinements are needed for these more complex metallic or highly coupled systems.

3. MBD in Extended Molecular Systems

Large, complex molecular systems, such as polymer melts and organic molecular solutions, offer a compelling platform for studying vdW interactions due to their structural complexity, which encompasses high conformational diversity, local density variations, void formation, and dynamic rearrangements.[42–44] We will hereon use the term extended to refer to such systems to emphasize their larger spatial extension when compared to dimer-like systems usually considered for the testing of approximations for vdW interactions. Here, we aim to a detailed examination of the collective effects of QDOs that underpin MBD in such extended system. We focus on high-performance polyethylene-based composites[45–48] as a prominent example of such

complexity. Carbon nanotubes and other nanoscale fillers are typically introduced to enhance mechanical strength and thermal conductivity,[49–52] and the polymer matrix, consisting primarily of repeating –CH_2– units, contacts the filler surfaces over large interfacial areas, rendering vdW interactions pivotal for effective load transfer and crack mitigation.[53,54] Understanding vdW forces in these large molecular systems is essential for predicting material properties in practical applications. At the same time, these systems can also serve as benchmark references that advance the development of computational models, capturing how atomistic interactions relate to the behavior of macroscopic materials.

To quantify the range and nature of many-body vdW forces in these large complex, molecular systems, we employed a systematic procedure integrating the generation of realistic structures with near ab initio parameterization of vdW interactions. For the polymer melts, we utilized structures generated using connectivity altering Monte Carlo (CAMC) simulations at 300 K, composed of 200 K atoms.[55] CAMC is a powerful simulation method that explores a wide range of conformational states by altering the connectivity of polymer chains through moves such as chain scission and rejoining.[56–58] This approach efficiently samples the polymer's configurational space, effectively capturing the diverse structural configurations, entanglements, and density variations inherent to polymer melts.[59] For benzene solutions, we initialized the structures and optimized them using the CHARMM force field, ensuring a broad sampling of the liquid-phase configurations for our purposes.[60] Methodological details regarding molecular structure generation can be found in Sect 6.1.

The starting point of our study in the differences between PW and many-body vdW interactions in polymer melt is to establish the minimal subsystem to be considered to accurately evaluate the force at a given atomic site. Our convergence tests revealed that the MBD method required about 1000 atomic neighbors—corresponding to a spherical region with a radius of 26 Bohr—to achieve a reliable force prediction. In contrast, PW vdW forces calculated within the most common first principles approaches (TS and D3[61,62]), require only ≈200 neighbors, that is, a region with a ≈13 Bohr radius (**Figure 3**(c)). We considered the D3 method, together with TS, to highlight that our analysis is not confined to the TS approach, but can be extended to any method that relies on the r^{-6} asymptotic power law. In other words, we will show that any method based on a PW potential, such as LJ, TS, D3, Exchange-dipole model[61,62] shares the same limitations

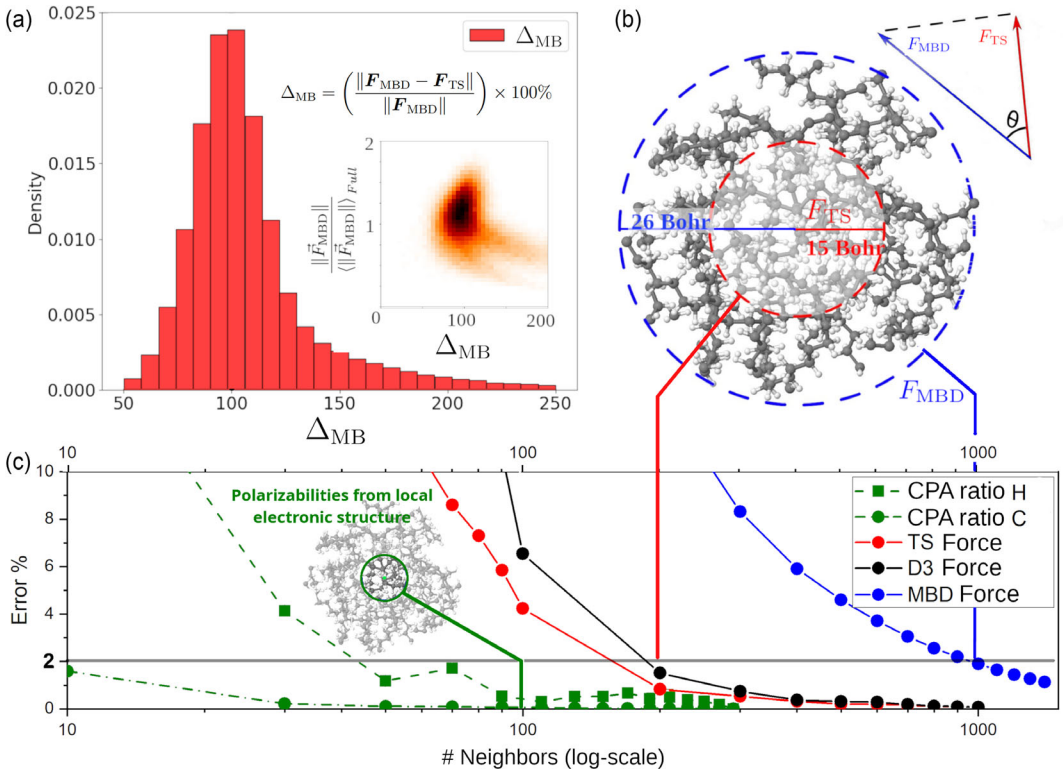

Figure 3. a) Distribution of percentage differences between MBD and TS vdW forces Δ_{MB} across the polymer melt system. The average Δ_{MB} value is 100%, indicating that MBD forces and the PW TS forces behave qualitatively differently. The inset shows a heatmap of the relative magnitudes of MBD forces versus the percentage differences, demonstrating that substantial differences are present across typical force magnitudes. b) Comparison of convergence ranges for vdW forces in the polymer melt using TS (red) and MBD (blue) methods. MBD forces converge over longer ranges (up to 26 Bohr or ≈1000 neighbors) compared to TS forces, which converge at about 15 Bohr (≈200 neighbors). c) Convergence of CPA ratios for hydrogen and carbon (dashed green lines) and vdW forces (red, black, and blue solid lines) as a function of the number of neighbors included in the calculations. Errors are expressed as percentages relative to a reference calculation with 3500 neighbors. The gray horizontal line marks our convergence criteria of 2% error. TS forces (red solid line) and D3 forces (black solid lines) converge at around 200 neighbors, while MBD forces (blue solid line) require about 1000 neighbors for convergence, reflecting the extended range of many-body vdW interactions in MBD.

when applied to extensive systems. In contrast, the stark difference in convergence behavior, illustrated in Figure 3(b), highlights how MBD interactions extend over considerably longer ranges than conventional PW approximations and reveals that collective many-body forces could significantly affect the system's predicted properties. Further details of the methodology employed to define convergence thresholds are presented in Sect. 6.2.

The broader range of MBD forces has important implications for modeling extended systems such as polymer melts and solutions. The enhanced reach of vdW interactions predicted by the MBD framework suggests that many-body effects could play a substantial role in determining the physical response of these systems. Properties such as viscosity, diffusion coefficients, and mechanical strength are sensitive to the range of molecular interactions. Neglecting these increased ranges of interactions due to many-body effects, as in traditional PW models, could lead to inaccuracies in predicted material properties and may necessitate reparameterization of force fields depending on the specific application.

The implications of these findings are further explored through an analysis of the MBD-TS force differences in the polymer melt system. The TS method, being a PW model that incorporates environment-dependent atomic properties, already contains information on the chemical environment thanks to the configuration specific parameterization of each QDO. This makes it a suitable baseline for comparison when assessing the relative differences arising specifically from many-body interactions not captured by PW frameworks. To quantify these differences, we define the percentage difference between the MBD and TS force vectors Δ_{MB} as

$$\Delta_{\mathrm{MB}} = \left(\frac{\|\mathbf{F}_{\mathrm{MBD}} - \mathbf{F}_{\mathrm{TS}}\|}{\|\mathbf{F}_{\mathrm{MBD}}\|} \right) \times 100\% \tag{7}$$

This metric captures both differences in magnitude and direction (angle) between the vdW force models. A percentage difference of $\approx$100% indicates that the magnitude of the difference between the TS and MBD forces is comparable to that of the MBD force itself.

Figure 3(a) shows this percentage difference Δ_{MB} distribution, which is centered at 100% with a standard deviation of 25% and long tails toward big values of Δ_{MB}. Such substantial differences are typical in systems with large conformational and topological variability. In polymer melts, the diverse configurations and complex topologies lead to significant deviations in vdW forces when comparing PW and many-body methods. While the dependance on topology in PW models is straightforward—interactions are based on PW distances—the MBD method involves complex coupling between quantum harmonic oscillators, making the influence of spatial arrangements more intricate and less predictable. The inset of Figure 3(a) shows a heatmap of relative MBD force magnitudes (force magnitudes divided by the average MBD force magnitude in the full system) versus Δ_{MB}, showing no direct correlation between the magnitude of the forces and their differences. This implies that large discrepancies between TS and MBD forces occur across all force magnitudes, not just in small or negligible forces.

Following our analysis of vdW force magnitudes and ranges, we examine the angular discrepancies and force modulus ratios between the TS and MBD methods $\|\mathbf{F}_{MBD}\|/\|\mathbf{F}_{TS}\|$ to identify general behaviors across different molecular systems. **Figure 4**(a) presents a polar heatmap that combines data from the polymer melt, benzene solution, and polyethylene dissolved in benzene systems. The radial axis represents the magnitude ratios $\|\mathbf{F}_{MBD}\|/\|\mathbf{F}_{TS}\|$ for each atom, while the angular axis represents the angle between the MBD and TS force vectors per atom. In this combined analysis, we observe distinct patterns based on atom types. The upper half of the polar plot corresponds to hydrogen atoms, and the lower half corresponds to carbon atoms. Hydrogen atoms generally exhibit higher force ratios, averaging around 2.5, indicating that the MBD method predicts forces $\approx$2.5 times stronger than the TS method for hydrogens. The angle differences for hydrogens are centered around 60 degrees but display a wide distribution, reflecting variability in directional discrepancies. In contrast, carbon atoms show force ratios closer to 1, suggesting similar force magnitudes between the methods, but their angle differences are centered around 70 degrees, indicating a greater but more consistent angular discrepancy compared to hydrogens.

In the benzene solution, our analysis also reveals distinctive behaviors between hydrogen and carbon atoms in terms of force ratios and percentage differences between the TS and MBD methods. As shown in Figure 4(b), hydrogen atoms exhibit a wider range of force ratios, generally around 2.5. Importantly, the percentage differences for hydrogen atoms are relatively small and concentrated, suggesting that while the force magnitudes differ, the directions of the forces predicted by TS and MBD are more closely aligned. In contrast, carbon atoms display a relatively concentrated force ratio around 0.5, meaning that the TS method predicts forces about twice as strong as MBD. However, the distribution of percentage differences for carbon atoms is wide, ranging from 75% to 300%. This significant spread in differences indicates that for carbon atoms, the primary discrepancies between the TS and MBD forces arise from differences in the directions (angles) of the forces rather than their magnitudes. The relatively consistent force ratios suggest that the magnitudes of the forces are similar between the methods for carbons, but the large discrepancies point to substantial angular deviations.

A definitive explanation for these contrasting behaviors between carbon and hydrogen atoms is not clear, as multiple factors—ranging from each atom's intrinsic polarizability to its immediate structural environment—contribute to how many-body screening manifests. While hydrogen atoms often lie at peripheral sites and may experience more pronounced local fluctuations, carbon atoms typically occupy network-forming backbones. Consequently, no single cause can fully account for the observed force ratio and angular discrepancies. Nonetheless, it is clear that the combination of different atomic polarizabilities and distinct local atomic environments strongly dictates how MBD forces differ from PW predictions.

In order to clarify these observations and expand our exploration of vDW interactions to a broader range of systems, we next turn to fullerenes.[63] By examining these highly symmetric carbon cages, we can evaluate how molecular symmetry influences the differences between the PW TS approach and the MBD method. Fullerenes, known for their characteristic molecular structures and varying degrees of symmetry,[64,65] thus serve as a straightforward platform for studying how symmetrical environments shape vdW force predictions. To that end, we performed molecular

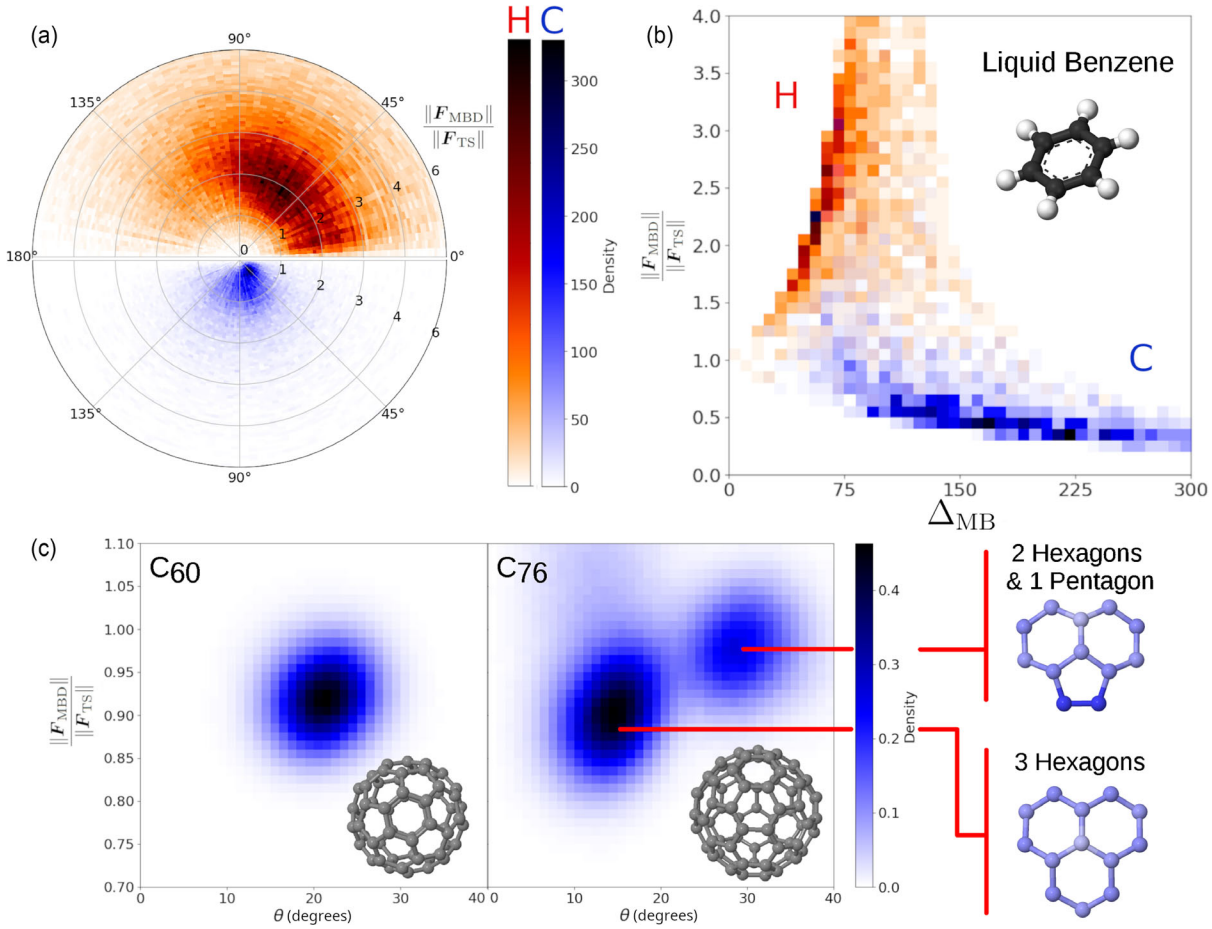

Figure 4. a) Polar heatmap of the ratio of MBD to TS force magnitudes $\|\mathbf{F}_{MBD}\|/\|\mathbf{F}_{TS}\|$ (radial axis) versus the angle between MBD and TS forces (angular axis), for hydrogens (top half, red) and carbons (bottom half, blue) for three systems on top of each other: polyethylene melt, polyethylene dissolved in benzene, and liquid benzene. Hydrogens exhibit an average force ratio of 2 (MBD forces are twice as strong as TS forces) with angles centered around 60 degrees. Carbons show force ratios below 1 (MBD forces are weaker than TS forces) with angles centered around 70 degrees. b) Heatmap of force ratio $\|\mathbf{F}_{MBD}\|/\|\mathbf{F}_{TS}\|$ versus percentage difference between MBD and TS forces for benzene, distinguishing hydrogens (red) and carbons (blue). Hydrogens display higher force ratios and lower percentage differences, while carbons exhibit lower force ratios and higher percentage differences, highlighting distinct behaviors between the two atom types. c) Left: Heatmap of force ratio $\|\mathbf{F}_{MBD}\|/\|\mathbf{F}_{TS}\|$ versus angle difference for the C_{60} fullerene. The Gaussian distribution reflects the perfect symmetry of C_{60}, resulting in uniform local environments and consistent force behavior between MBD and TS methods. Right: Heatmap of force ratio versus angle difference for C_{76} fullerene. The bimodal distribution arises from multiple local symmetries in C_{76}, leading to different MBD responses. The two peaks correspond to angle differences of ≈13 degrees and 30 degrees, indicating variations in force directions due to the differing local atomic arrangements.

dynamics simulations of C_{60} and C_{76} at 300 K using DFTB+.[66] In C_{60}, each carbon atom occupies an equivalent local environment reflecting its high degree of symmetry, whereas C_{76} features multiple distinct atomic neighborhoods consistent with its more complex geometry (see Figure 2(b)).

Figure 4(c) provides heatmaps illustrating the relationship between the force ratio $\|\mathbf{F}_{MBD}\|/\|\mathbf{F}_{TS}\|$ and the angle between the MBD and TS force vectors for C_{60} and C_{76}, respectively. For C_{60} (Figure 4(c)), the heatmap displays a single, concentrated cluster with a force ratio close to 0.93 and angle differences centered around 20 degrees. This indicates a consistent level of discrepancy between the TS and MBD forces due to the uniform atomic environments. The forces predicted by both methods are similar in both magnitude and direction across all atoms, reflecting the high symmetry of the molecule. In contrast, the heatmap for C_{76} reveals two distinct clusters, showcasing the influence of its lower symmetry and varied atomic environments. One cluster shows a force ratio around 0.90 and small angle differences, (≈15 degrees) suggesting regions where the TS and MBD forces are well-aligned. The other cluster has a force ratio close to 1.0 and larger angle differences (cosine of ≈0.87, angle difference of about 30 degrees), indicating regions with more significant discrepancies in force directions between the two methods. Furthermore, these regions with a larger angle difference are caused by less symmetrical carbon configurations, composed of single pentagons embedded in the hexagonal carbon patterns. These variations illustrate how even the very simple and restricted configurational diversity in C_{76} leads to complex manifestations of many-body effects not captured uniformly by PW models.

This pattern mirrors our observations in large molecular systems like polymer melts and benzene solutions, where the lack of uniform symmetry and diverse local environments lead to significant discrepancies between TS and MBD forces, primarily manifested through angle differences. In these systems, the variability in atomic arrangements and conformations results in complex many-body interactions that are not adequately captured by PW methods. Just as the reduced symmetry in C_{76} amplifies the differences between TS and MBD predictions, the disorder and conformational diversity in extended systems appears to accentuate the impact of many-body effects.

4. vdW Interaction Range and Collective Vibrations

Many-body interactions significantly influence the vDW decay rates between constituents of a system, with the extent of these effects depending on the local atomic arrangements and molecular topology.[22,67] To qualitatively understand the differences between the PW TS method and the MBD method, we examine how modifying the power-law decay exponent in the TS model can capture aspects of many-body interactions in extended systems.

We introduce a correction to the TS forces by adjusting the decay rate exponent based on interatomic distances. For any atom j within a molecular system of N atoms, the modified force $\widetilde{\boldsymbol{F}}^{j}$ is defined as

$$\widetilde{\boldsymbol{F}}^{\mathrm{j}} = \sum_{i=1}^{\mathrm{N}} \boldsymbol{F}_{\mathrm{TS}}^{\mathrm{ij}} \left(\frac{r_{\mathrm{ij}}}{R_0}\right)^{\alpha_0 + \alpha_1(\mathrm{R_0}/\mathrm{r_{ij}})} \tag{8}$$

where $\boldsymbol{F}_{\mathrm{TS}}^{\mathrm{ij}}$ is the PW TS force between atoms i and j, r_{ij} is their interatomic distance, R_0 is a characteristic length scale, and α_0 and α_1 are parameters that adjust the decay exponent to reflect the influence of many-body effects. The term α_0 captures the baseline long-range decay rate correction due to the molecular environment, while α_1 accounts for changes in the decay rate at shorter distances due to atomic proximity.

We calibrated the parameters R_0, α_0, and α_1, using datasets from large molecular systems, such as polymer melts and benzene solutions. The fitting aimed to match MBD forces and capture its extended interaction range, recognizing that angular discrepancies will remain due to the lack of angular dependance in our correction model. The aggregate fitted parameters are presented in **Table 1**.

The parameter α_0 represents the baseline correction to the decay exponent for long-range interactions, a systematic alteration of the vdW force decay rate due to many-body effects. Specifically, with $\alpha_0 = 1.71$, the effective force decay exponent is reduced from the PW value of -7 to ≈ -5.3 (calculated as $-7 + \alpha_0 = -7 + 1.71 = -5.29$), corresponding to a decrease of about 24%. This significant reduction in the decay exponent leads to the extended interaction ranges observed in the MBD forces.

Table 1. Fitted parameters used in the decay rate correction model.

Parameter	Value	Relative Variability [%]
R_0 (Bohr)	3.91 ± 0.15	3.83
α_0	1.71 ± 0.17	9.94
α_1	-8.00 ± 2.00	25.00

In terms of the practical application of this method, using a single, ensemble-averaged decay exponent adds no extra computational cost over the standard TS scheme, and no additional operations are incurred once the exponent is fixed. But if one wishes to tune the exponent locally—for example, per atom's chemical environment—the dispersion routine would need to retrieve (or compute) an exponent for each atom. Nevertheless, because the functional form is still PW, the exponents could be pretabulated or predicted on-the-fly by a light-weight machine-learning model trained on local structural descriptors, keeping the overall overhead negligible. Simultaneously, as the current modification only affects the distance-dependent factor, the decay-corrected TS term can be incorporated into calculations with periodic boundary conditions. Following the fitted parameters, we would have to reduce the vdW force-law exponent from -7 to ≈ -5.3, and the corresponding energy exponent from -6 to -4.3. This is still steeper than the -3 threshold required for absolute convergence in 3D lattices, so a real-space cutoff can be employed with only a modest increase in its radius. Alternatively, one may maintain the usual Ewald or PME lattice sum and simply apply the same adjusted exponent to every atom pair (i,j). In this context, the asymptotic scaling remains $O(N \log N)$ (for Ewald/PME) or $O(N)$ (for a finite cutoff), enabling the method to be adapted to molecular crystals or layered 2-D materials after suitable parameter tuning.

By examining the interaction ranges obtained from the polymer melt shown in Figure 3(b), and assuming a PW decomposition of the MBD force, we can perform a simple calculation to estimate the effective decay exponent required to reproduce these predicted interaction ranges. The TS forces converge at around 13 Bohr with a decay exponent of -7, while the MBD forces converge at $\approx$26 Bohr. Using the relationship between interaction range and decay exponent, we find that an effective decay exponent of about -5.5 is needed to achieve the MBD interaction range. This estimation is consistent with the decay exponent implied by our fitted α_0 (-5.3), reinforcing the conclusion that many-body effects result in a reduced decay rate and extended vdW interaction ranges, and that the long-range correction captured by α_0 effectively represents the long-range influence of many-body effects on the decay behavior of vdW forces in large molecular systems.

In contrast, the higher relative variability of 25% in α_1 indicates that this parameter is less precisely determined in our fitting procedure. This higher variability in α_1 can be attributed to the significant variations in local atomic conformations inherent in disordered systems like polymer melts and benzene solutions. The local environments in these systems are highly diverse, with atoms experiencing a wide range of neighboring configurations. The MBD method is sensitive to these local structural differences due to its explicit treatment of many-body interactions.

A single parameter like α_1 is insufficient to capture this complex variability in short-range decay behavior without considering angular dependencies. The lack of explicit angle dependance in our decay rate correction model limits its ability to account for

discrepancies in angle which arise from many-body interactions. This suggests that to accurately model the short-range many-body effects and improve the fitting of α_1, it is necessary to incorporate angular corrections that reflect the vector nature of the forces and the influence of molecular topology.

Our analysis shows that adjusting the decay exponent in the TS model using this correction effectively accounts for a significant portion of the differences in force magnitudes between the TS and MBD methods. Specifically, in the large molecular systems we studied, the correction reduced the average discrepancy in force magnitudes by ≈60%. This suggests that the majority of the many-body contributions can be represented through changes in the interaction decay rate. This effectiveness is illustrated in **Figure 5**(c), which displays heatmaps of the relative MBD force versus the difference between TS and MBD forces in the polymer melts, both before (red) and after (blue) applying the decay rate correction. The significant reduction in force discrepancies across all magnitudes after the correction demonstrates how adjusting the decay rate exponent brings the PW force predictions into closer agreement with those of the MBD method.

However, the lack of explicit angular dependance in our correction model introduces a limitation. While the decay rate correction improves the agreement in force magnitudes, it does not capture the noncollinear nature of the forces arising from many-body interactions. This suggests that incorporating angular dependencies and considering the complex interplay between many-body effects and molecular topology may be necessary to fully reconcile the differences between PW and many-body methods.[68] The impact of many-body interactions extends beyond force magnitudes to dynamical properties such as vibrational spectra. We analyzed this effect in larger fullerenes, specifically C_{720}, because many-body interactions are known to become more pronounced with increasing system size.[25,26,69] Figure 5(a) shows the power spectra obtained from molecular dynamics simulations of C_{720} at 300 K using DFTB+, comparing the MBD method (blue curve) and the TS method (red curve). The lowest vibrational mode, highlighted by the red rectangle, exhibits significantly higher intensity in the MBD spectrum compared to TS, indicating that MBD predicts enhanced collective (low-frequency) vibrations as a consequence of the extended interaction range and coupling between vdW interactions and structure deformations resulting from many-body effects.[25] This enhancement underscores how many-body interactions become increasingly significant in larger systems, affecting the vibrational properties and highlighting the limitations of PW models in such contexts. The MBD-induced shifts we observe for C_{720} would, in principle, translate into measurable IR/Raman peak shifts and/or intensity changes for low-frequency cage modes in large fullerenes; however, verifying these shifts experimentally in these systems is presently challenging because bulk quantities of such large fullerenes are difficult to synthesize.[70] We therefore treat C_{720} purely as a theoretical benchmark for size-dependent many-body effects.

Further evidence is presented in Figure 5(b), which provides zoomed-in power spectra of the lowest vibrational mode in C_{320} at 200 K (top) and 400 K (bottom), again comparing MBD (blue)

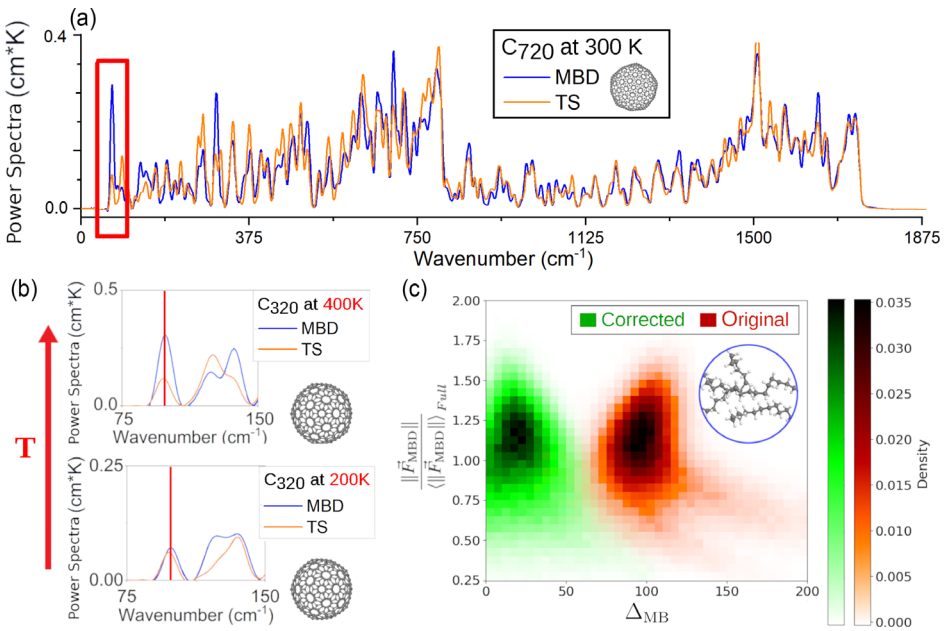

Figure 5. a) Power spectra obtained from molecular dynamics simulations of C_{720} at 300 K using DFTB+, comparing the MBD method (blue curve) and the PW TS method (orange curve). The lowest vibrational mode, highlighted by the red rectangle, shows significantly higher intensity in the MBD spectrum compared to TS, indicating that MBD predicts enhanced collective vibrations. b) Zoomed-in power spectra of the lowest vibrational mode in C_{320} at 400 K (top) and 200 K (bottom), comparing MBD (blue) and TS (orange) methods. As the temperature increases, the excitation of this mode becomes more pronounced in the MBD spectra, demonstrating the temperature-dependent enhancement of collective vibrations captured by MBD. c) Heatmaps of Δ_{MB} versus the difference between TS and MBD forces, both before (red) and after (blue) applying the decay rate correction to the polymer melts. The significant reduction in force discrepancies after the correction across all magnitudes illustrates the effectiveness of the decay rate correction in improving TS force predictions toward MBD.

and TS (orange) methods. We chose C_{320} to demonstrate that even in smaller systems, temperature plays a critical role in influencing vibrational spectra. As the temperature increases, the molecular configurations become more disordered due to enhanced thermal motion, leading to a broader sampling of conformations and increased structural fluctuations. Consequently, the excitation of the lowest vibrational mode becomes more pronounced in the MBD spectra at higher temperatures. This temperature-dependent enhancement of collective vibrations captured by MBD—but not by TS—highlights the significance of many-body effects in modeling vibrational properties, which are sensitive to both the system size and thermal fluctuations.

These findings emphasize that while modifying the decay rate exponent in PW models can capture key aspects of many-body effects in force magnitudes, it is insufficient to account for the directional and collective phenomena arising from many-body interactions, which nontrivially depend on system sizes and temperatures. The discrepancies in vibrational spectra and the inability of the decay rate correction to capture the enhanced collective vibrations suggest that future models need to incorporate angular dependencies and consider the complex interplay between many-body interactions and molecular topology.

5. Conclusions

While energies provide information about the stability and equilibrium configurations of systems, forces determine the response of systems to perturbations and drive the evolution of molecular structures. Therefore, accurate force predictions become crucial to describe the collective properties of systems lacking strong covalent bonding. Further understanding of the system dependance of vdW forces will thus enhance the reliability of theoretical predictions for complex extended molecular systems. By comparing the PW TS method with the MBD method across systems such as polymer melts, benzene solutions, and fullerenes, we showed that MBD interactions can strongly influence long-range forces, both in magnitude and direction, in large molecular systems.

Our analysis revealed that many-body effects can lead to a reduction of ≈25% in the vdW decay rate exponent compared to the PW −7 force decay rate for large molecular systems. This reduced decay rate results in extended interaction ranges, with MBD forces converging over distances up to 26 Bohr—approximately twice the range required for TS forces in polymer melts. Such extended ranges can significantly affect material properties dependent on long-range interactions, such as elasticity and mechanical strength. The longer reach of vdW forces in the MBD framework suggests that many-body effects contribute to the collective behavior of materials, potentially enhancing their elastic response by facilitating force transmission over greater distances.

Our study on fullerenes highlighted the role of molecular symmetry in vdW force predictions. In highly symmetric systems like C_{60}, the uniform atomic environments lead to relatively consistent force predictions between TS and MBD methods, with smaller discrepancies in both magnitude and direction. This suggests that in symmetric, ordered systems, PW models may suffice for certain applications. Conversely, marginally less symmetric systems like C_{76} exhibit much greater discrepancies due to their multiple local atomic environments, resulting in more pronounced many-body effects.

Furthermore, our analysis of the vibrational spectra of large fullerenes revealed that many-body interactions significantly impact vibrational dynamics. In systems like C_{720}, the enhanced collective vibrations observed in the MBD method highlight the critical role of many-body effects in modifying low-frequency vibrational modes. These collective vibrations are a consequence of the extended interaction ranges and altered decay resulting from many-body interactions. The discrepancy in vibrational spectra between TS and MBD becomes more pronounced with increasing system size and depends on temperature, as demonstrated by our studies on C_{320}. Elevated temperatures lead to increased thermal motion and structural fluctuations, promoting the manifestation of many-body effects.

By extending these insights to disordered systems like polymer melts and benzene solutions, we observe that the lack of uniform symmetry and the diversity of local environments amplify the differences between TS and MBD forces. The complex molecular topologies and conformations in these systems lead to significant variations in force magnitudes and directions that are not captured by PW models. This emphasizes the necessity of incorporating many-body effects to accurately predict properties such as elasticity, viscosity, and diffusion coefficients in materials.

6. Computational Methods

6.1. Molecular Structure Generation

For both the benzene–polymer mixture and liquid benzene structures, the CHARMM-GUI Polymer Builder[71,72] was used at 300 K to initialize systems under near-ambient conditions. Benzene was selected as the solvent in step 2 of the CHARMM-GUI workflow, prompting the construction of a rectangular $100 \times 100 \times 100$ Å simulation box with a target number of benzene molecules to approximate a liquid density of 0.88 g cm^{-3}. In the benzene–polymer mixtures, 100 polyethylene chains were introduced, each comprising 302 atoms, leading to 30,200 total polymer atoms. The ratio of benzene to polymer was fixed at 1:3, thereby achieving a composition conducive to partial solvation. Throughout this procedure, the CHARMM General Force Field (CGenFF) was employed, assigning bonded parameters (bonds, angles, torsions) and nonbonded interactions (LJ plus partial charges) for both benzene and polymer segments. Standard polyethylene building blocks were automatically recognized within CGenFF, ensuring consistent parameterization without the need for manual fragment specification.

After specifying the system shape and dimensions in CHARMM-GUI, coordinate and topology files were produced, distributing benzene molecules and polymer chains so as to minimize initial overlaps. A short energy equilibration was then performed (step 3) to relieve any unfavorable steric contacts. Subsequent equilibration (step 4) occurred in the NVT ensemble at 300 K, gradually shifting from a softened nonbonded potential (e.g., Weeks–Chandler–Andersen) to the full CGenFF nonbonded interactions. During this process, a Langevin integrator was employed for 200 000 molecular dynamics steps with a time step of 0.050 ps, enabling stable relaxation of the system.

Pure polymer melt configurations were created using CAMC simulations at normal conditions of pressure and temperature.[56–58] This procedure modifies polymer connectivity through moves such as chain scission or rejoining, allowing the polymer chains to efficiently sample a broad range of conformational states while preserving essential intramolecular degrees of freedom. A periodic unit cell containing 300050 atoms was obtained with polyethylene chains spanning 12002 atoms each. This provided sufficiently diverse structural configurations for subsequent semi-empirical calculations.

For the polyethylene melts and benzene solutions, once classical equilibration was complete, the relevant charge population analysis (CPA) ratios (later employed in TS and MBD calculations) were extracted from single-point quantum-mechanical computations in the DFTB + software.[66] The 3ob-3-1 Slater–Koster parameter set was used to accurately describe the organic compositions of carbon and hydrogen, applying a self-consistent charge tolerance of 1×10^{-7}. Next, vdW-only interactions were incorporated through three different dispersion schemes, each following a damping function compatible with the DFTB+ implementation. The first approach involved a PW D3 correction from the simple-dftd3[73] package, relying on empirically derived C_6 coefficients and an exponential damping function optimized for DFTB+. The second employed the MBD method through libmbd[74] under the range-separated self-consistent screening (rsSCS) method. Finally, a Python-based implementation[75] of the TS model was used, mirroring the established TS approach in DFTB+ yet allowing additional control over parameters to facilitate the specialized analysis of decay rate modification.

All DFTB and vdW-only calculations were executed on a local high-performance computing cluster to handle the large number of configurations and the computational overhead of systematic comparisons between PW and MBD treatments. Throughout the simulations, periodic boundary conditions were imposed where appropriate (e.g., polymer melts), while smaller or nonperiodic systems (e.g., isolated molecules, fragments) were treated with vacuum boundary conditions in DFTB+.

6.2. Determination of Ranges of Interaction

For each generated structure, Density Functional Tight Binding (DFTB+) single-point calculations were employed to obtain CPA ratios for the atoms within the system.[76–78] DFTB is a semi-empirical approach rooted in density functional theory (DFT)[79–81] that relies on a parameterization scheme referencing ab initio calculations while retaining a minimal basis set, thus considerably reducing computational overhead compared to pure DFT methods. Despite this reduced basis, DFTB has demonstrated reliable performance for an array of organic molecules, molecular crystals, surfaces, and nanomaterials,[82] enabling practical large-scale simulations without sacrificing key quantum-mechanical aspects. In particular, the CPA ratios derived from DFTB+ effectively capture local electronic environment shifts by approximating partial charges for each atom, echoing the successes highlighted by Stöhr et al.[83] in reproducing Hirshfeld-like volume partitions. These CPA ratios thus incorporate environment-dependent modifications to atomic polarizabilities and dispersion coefficients needed for properly modeling vdW interactions in the MBD and TS methods.

To ensure convergence of the CPA ratios, for each one of our structures, our calculations were centered on selected atoms at random with a neighbor list encompassing 400 atoms. We systematically reduced the neighbor list size and calculated the CPA ratio errors with respect to a reference calculation using 400 atoms. As shown in Figure 3(c), considering 100 neighbors for the CPA ratio calculation was sufficient, achieving an error below 2%. This approach allows us to efficiently parameterize vdW interactions while maintaining computational efficiency.

After obtaining the converged CPA ratios, our next step was to establish a reference for vdW force convergence in the large molecular systems. We calculated the vdW forces using an extensive neighbor list of up to 3500 atoms for a given central atom, ensuring that all significant contributions were included. This calculation served as our benchmark reference force for convergence. We then incrementally reduced the size of the neighbor list and recalculated the vdW force vectors at each step. By comparing these forces with the reference forces, we quantified the convergence of the vdW interactions. Specifically, we computed the magnitude of the vector difference between the forces at each step and the reference force, continuing this process until the change was ≈2%—our defined convergence criterion (see Figure 3(c)). This procedure was applied consistently for the TS, MBD, and D3[84,85] dispersion approaches. In particular, D3 relies on a predominantly PW additivity framework—supplemented by an optional three-body Axilrod–Teller–Muto term—[86,87] to approximate some many-atom effects. Unlike MBD, which fully incorporates collective quantum oscillators, the D3 method primarily tabulates C_6 coefficients for each atom pair and applies an empirical damping function. Specifically, we employed the the D3(Becke–Johnson) [D3(BJ)] dispersion correction, which employs a Becke–Johnson–type damping function for improved accuracy in describing mid-range interactions.[85] In practice, D3(BJ) modifies the original D3 short-range damping. This variant comes packaged within the DFTB+ library, enabling a straightforward incorporation of D3(BJ) dispersion terms via internal parameters and damping functions fitted specifically to DFTB settings.

Acknowledgements

The authors are grateful for the support of the Luxembourg National Research Fund (C20/MS/14782078/QuaC). The authors extend their thanks to Ariadni Boziki for the many fruitful discussions they had about the topics of this paper. The calculations presented in this paper were carried out using the HPC facilities of the University of Luxembourg. The authors gratefully acknowledge Prof. Doros N. Theodorou, Loukas Peristeras, Stefanos D. Anogiannakis and the Computational Materials Science and Engineering Group at the National Technical University of Athens for providing the CAMC polyethylene melt structures used in this study. Their contributions significantly aided the advancement of this research.

Conflict of Interest

The authors declare no conflict of interest.

Data Availability Statement

The data that support the findings of this study are openly available in GitHub at https://github.com/iansosa/QC-Toolkit, reference number 1.

Keywords

density functional tight binding, large molecular systems, many-body dispersion, nanostructures, polymer melts, van der Waals

Received: April 9, 2025
Revised: June 11, 2025
Published online:

[1] J. N. Israelachvili, *Intermolecular And Surface Forces*, Academic Press, San Diego, CA **2011**.
[2] A. J. Stone, *The Theory Of Intermolecular Forces*, Oxford University Press, Oxford, UK **2013**.
[3] Y. Liu, Y. Huang, X. Duan, *Nature* **2019**, *567*, 323.
[4] K. Autumn, M. Sitti, Y. A. Liang, A. M. Peattie, W. R. Hansen, S. Sponberg, T. W. Kenny, R. Fearing, J. N. Israelachvili, R. J. Full, *Proc. Natl. Acad. Sci. U. S. A.* **2002**, *99*, 12252.
[5] K. A. Dill, *Biochemistry* **1990**, *29*, 7133.
[6] V. A. Parsegian, *Van Der Waals Forces: A Handbook For Biologists, Chemists, Engineers, And Physicists*, Cambridge University Press, Cambridge, UK **2006**.
[7] A. K. Geim, K. S. Novoselov, *Nat. Mater.* **2007**, *6*, 183.
[8] J. F. Dobson, T. Gould, *J. Phys.: Condens. Matter* **2012**, *24*, 073201.
[9] J. Hermann, R. A. DiStasio Jr., A. Tkatchenko, *Chem. Rev.* **2017**, *117*, 4714.
[10] T. Bučko, J. Hafner, S. Lebègue, J. G. Ángyán, *J. Phys. Chem. A* **2010**, *114*, 11814.
[11] S. Grimme, *J. Comput. Chem.* **2004**, *25*, 1463.
[12] G. Hu, C. Q. Chen, K. T. Ramesh, J. W. McCauley, *Acta Mater.* **2012**, *60*, 3480.
[13] T. Hochrainer, S. Sandfeld, M. Zaiser, P. Gumbsch, *J. Mech. Phys. Solids* **2014**, *63*, 167.
[14] E. Van der Giessen, A. Needleman, *Mater. Sci. Eng.* **1995**, *3*, 689.
[15] V. S. Deshpande, A. Needleman, E. Van der Giessen, *Acta Mater.* **2002**, *50*, 831.
[16] J. Klimeš, A. Michaelides, *J. Chem. Phys.* **2012**, *137*, 120901.
[17] A. Ambrosetti, D. Alfè, R. A. DiStasio Jr., A. Tkatchenko, *J. Phys. Chem. Lett.* **2014**, *5*, 849.
[18] S. Grimme, *Mol. Sci.* **2011**, *1*, 211.
[19] A. M. Reilly, A. Tkatchenko, *J. Phys. Chem. Lett.* **2013**, *4*, 1028.
[20] N. Marom, R. A. DiStasio Jr., V. Atalla, S. Levchenko, A. M. Reilly, J. R. Chelikowsky, L. Leiserowitz, A. Tkatchenko, *Angew. Chem. Int. Ed.* **2013**, *52*, 6629.
[21] A. Tkatchenko, R. A. DiStasio Jr., R. Car, M. Scheffler, *Phys. Rev. Lett.* **2012**, *108*, 236402.
[22] A. Ambrosetti, A. M. Reilly, R. A. DiStasio Jr., A. Tkatchenko, *J. Chem. Phys.* **2014**, *140*, 18A508.
[23] A. M. Reilly, A. Tkatchenko, *J. Chem. Phys.* **2013**, *139*, 024705.
[24] A. Tkatchenko, A. Ambrosetti, R. A. DiStasio Jr., *J. Chem. Phys.* **2013**, *138*, 074106.
[25] P. Hauseux, T. T. Nguyen, A. Ambrosetti, K. S. Ruiz, S. P. A. Bordas, A. Tkatchenko, *Nat. Commun.* **2020**, *11*, 1651.
[26] A. Ambrosetti, N. Ferri, R. A. DiStasio Jr., A. Tkatchenko, *Science* **2016**, *351*, 1171.
[27] A. I. Vakis, V. A. Yastrebov, J. Scheibert, L. Nicola, D. Dini, C. Minfray, A. Almqvist, M. Paggi, S. Lee, G. Limbert, J. F. Molinari, G. Anciaux, R. Aghababaei, S. E. Restrepo, A. Papangelo, A. Cammarata, P. Nicolini, C. Putignano, G. Carbone, S. Stupkiewicz, J. Lengiewicz, G. Costagliola, F. Bosia, R. Guarino, N. M. Pugno, M. H. Müser, M. Ciavarella, *Tribol. Int.* **2018**, *125*, 169.
[28] X. Wang, Z. Kou, R. Qiao, Y. Long, B. Li, X. Li, W. Guo, X. Liu, J. Yin, *Nat. Commun.* **2025**, *16*, 324.
[29] A. M. Reilly, A. Tkatchenko, *Phys. Rev. Lett.* **2014**, *113*, 055701.
[30] A. Ambrosetti, P. Umari, P. L. Silvestrelli, J. Elliott, A. Tkatchenko, *Nat. Commun.* **2022**, *13*, 813.
[31] R. J. Maurer, C. Freysoldt, A. M. Reilly, J. G. Brandenburg, O. T. Hofmann, T. Björkman, S. Lebègue, A. Tkatchenko, *Annu. Rev. Mater. Res.* **2019**, *49*, 1.
[32] A. Tkatchenko, M. Scheffler, *Phys. Rev. Lett.* **2009**, *102*, 073005.
[33] F. L. Hirshfeld, *Theor. Chim. Acta* **1977**, *44*, 129.
[34] A. Khabibrakhmanov, D. V. Fedorov, A. Tkatchenko, *J. Chem. Theory Comput.* **2023**, *19*, 7895.
[35] P. Jurečka, J. Šponer, J. Černỳ, P. Hobza, *Phys. Chem. Chem. Phys.* **2006**, *8*, 1985.
[36] G. H. Golub, C. F. Van Loan, *Matrix Computations*, Johns Hopkins University Press, Baltimore, MD **2013**.
[37] J. Demmel, *Applied Numerical Linear Algebra*, SIAM, Philadelphia, PA **1997**.
[38] M. Stöhr, T. Van Voorhis, A. Tkatchenko, *Chem. Soc. Rev.* **2019**, *48*, 4118.
[39] M. Kim, W. J. Kim, T. Gould, E. K. Lee, S. Lebègue, H. Kim, *J. Am. Chem. Soc.* **2020**, *142*, 2346.
[40] J. Hermann, A. Tkatchenko, *Phys. Rev. Lett.* **2020**, *124*, 146401.
[41] J. F. Dobson, A. Ambrosetti, *J. Chem. Theory Comput.* **2023**, *19*, 6434.
[42] J.-P. Hansen, I. R. McDonald, *Theory Of Simple Liquids*, Academic Press, San Diego, CA **2013**.
[43] M. Mehdikhani, L. Gorbatikh, I. Verpoest, S. V. Lomov, *J. Compos. Mater.* **2018**, *53*, 1579.
[44] F. C. Kalutantirige, J. He, L. Yao, S. Cotty, S. Zhou, J. W. Smith, E. Tajkhorshid, C. M. Schroeder, J. S. Moore, H. An, X. Su, Y. Li, Q. Chen, *Nat. Commun.* **2024**, *15*, 2852.
[45] Y. Li, Y. Liu, X. Peng, C. Yan, S. Liu, N. Hu, *Comput. Mater. Sci.* **2011**, *50*, 1854.
[46] A. P. Awasthi, D. C. Lagoudas, D. C. Hammerand, *Mater. Sci. Eng.* **2009**, *17*, 015002.
[47] S. J. V. Frankland, V. M. Harik, *Surf. Sci.* **2003**, *525*, L103.
[48] A. Karatrantos, R. J. Composto, K. I. Winey, M. Kröger, N. Clarke, *Polymers* **2019**, *11*, 876.
[49] G. H. Michler, H.-H. Kausch-Blecken von Schmeling, *Polymer* **2013**, *54*, 3131.
[50] M. J. Biercuk, M. C. Llaguno, M. Radosavljevic, J. K. Hyun, A. T. Johnson, J. E. Fischer, *Appl. Phys. Lett.* **2002**, *80*, 2767.
[51] P. M. Ajayan, L. S. Schadler, C. Giannaris, A. Rubio, *Adv. Mater.* **2000**, *12*, 750.
[52] M. S. P. Shaffer, A. H. Windle, *Adv. Mater.* **1999**, *11*, 937.
[53] *Woodhead Publishing Series In Composites Science And Engineering* (Eds: T. Tam, A. Bhatnagar, In A. Bhatnagar) Woodhead Publishing, Cambridge, UK **2016**, 1–39.
[54] S. M. Kurtz, *The UHMWPE Handbook*, Academic Press, San Diego, CA **2004**.
[55] Computational Materials Science and Engineering Group, National Technical University of Athens, Athens, Greece, Polyethylene Melt CAMC Configuration Dataset, 2024 (courtesy communication)
[56] P. V. K. Pant, D. N. Theodorou, *Macromolecules* **1995**, *28*, 7224.
[57] N. C. Karayiannis, V. G. Mavrantzas, D. N. Theodorou, *Phys. Rev. Lett.* **2002**, *88*, 105503.
[58] *Bridging Time Scales: Molecular Simulations For The Next Decade* (Eds: D. N. Theodorou, In P. Nielaba, M. Mareschal, G. Ciccotti), Springer-Verlag, Berlin, Germany **2002**, pp. 67–88.

[59] C. Peter, K. Kremer, *Soft Matter* **2009**, *5*, 4357.
[60] B. R. Brooks, C. L. I. Brooks, A. D. J. Mackerell, L. Nilsson, R. J. Petrella, B. Roux, Y. Won, G. Archontis, C. Bartels, S. Boresch, A. Caflisch, L. M. Caves, A. Cui, A. R. Dinner, M. Feig, S. Fischer, J. Gao, M. Hodoscek, W. Im, K. Kuczera, T. Lazaridis, J. Ma, V. Ovchinnikov, E. Paci, R. W. Pastor, C. B. Post, J. Z. Pu, M. Schaefer, B. Tidor, R. M. Venable, et al., *J. Comput. Chem.* **2009**, *30*, 1545.
[61] A. D. Becke, E. R. Johnson, *J. Chem. Phys.* **2006**, *124*, 014104.
[62] A. D. Becke, E. R. Johnson, *J. Chem. Phys.* **2005**, *123*, 154101.
[63] B. Liu, J. Jin, M. Liu, *Mater.* **2024**, *10*, 227.
[64] M. Švec, P. Merino, Y. J. Dappe, C. González, E. Abad, P. Jelnek, J. A. Martn-Gago, *Phys. Rev. B* **2012**, *86*, 121407(R).
[65] G. B. Adams, M. O'Keeffe, R. S. Ruoff, *J. Phys. Chem.* **1994**, *98*, 9465.
[66] B. Hourahine, B. Aradi, V. Blum, F. Bonafé, A. Buccheri, C. Camacho, C. Cevallos, M. Y. Deshaye, T. Dumitrică, A. Dominguez, S. Ehlert, M. Elstner, T. van der Heide, J. Hermann, S. Irle, J. J. Kranz, C. Köhler, T. Kowalczyk, T. Kubař, I. S. Lee, V. Lutsker, R. J. Maurer, S. K. Min, I. Mitchell, C. Negre, T. A. Niehaus, A. M. N. Niklasson, A. J. Page, A. Pecchia, G. Penazzi, et al., *J. Chem. Phys.* **2020**, *152*, 124101.
[67] M. Galante, A. Tkatchenko, *Phys. Rev. Res.* **2023**, *5*, L012028.
[68] Z. Shen, R. I. Sosa, J. Lengiewicz, A. Tkatchenko, S. P. A. Bordas, *ArXiv preprint arXiv:2503.15149* **2025**.
[69] Z. Shen, R. I. Sosa, S. P. A. Bordas, A. Tkatchenko, J. Lengiewicz, *Int. J. Eng. Sci.* **2024**, *204*, 104126.
[70] M. Mojica, J. A. Alonso, F. Méndez, *J. Phys. Org. Chem.* **2013**, *26*, 526.
[71] S. Jo, T. Kim, V. G. Iyer, W. Im, *J. Comput. Chem.* **2008**, *29*, 1859.
[72] Y. K. Choi, S.-J. Park, S. Park, S. Kim, N. R. Kern, J. Lee, W. Im, *J. Chem. Theory Comput.* **2021**, *17*, 2431.
[73] S. Ehlert, simple-dftd3, Version 1.2.1, 2024; GitHub repository, https://github.com/dftd3/simple-dftd3.
[74] J. Hermann, libMBD, Version 0.12.8, 2024; GitHub repository, https://github.com/libmbd/libmbd.
[75] R. I. Sosa, QC-Toolkit, Version 1.0, 2025; GitHub repository, https://github.com/iansosa/QC-Toolkit.
[76] D. Porezag, T. Frauenheim, T. Köhler, G. Seifert, R. Kaschner, *Phys. Rev. B* **1995**, *51*, 12947.
[77] M. Elstner, D. Porezag, G. Jungnickel, J. Elsner, M. Haugk, T. Frauenheim, S. Suhai, G. Seifert, *Phys. Rev. B* **1998**, *58*, 7260.
[78] M. Elstner, G. Seifert, *Philos. Trans. R. Soc. A* **2014**, *372*, 20120483.
[79] P. Hohenberg, W. Kohn, *Phys. Rev.* **1964**, *136*, B864.
[80] W. Kohn, L. J. Sham, *Phys. Rev.* **1965**, *140*, A1133.
[81] R. O. Jones, *Rev. Mod. Phys.* **2015**, *87*, 897.
[82] F. Spiegelman, N. Tarrat, J. Cuny, L. Dontot, E. Posenitskiy, C. Mart, A. Simon, M. Rapacioli, *Adv. Phys. X* **2020**, *5*, 1710252.
[83] M. Stöhr, G. S. Michelitsch, J. C. Tully, K. Reuter, R. J. Maurer, *J. Chem. Phys.* **2016**, *144*, 151101.
[84] S. Grimme, J. Antony, S. Ehrlich, H. Krieg, *J. Chem. Phys.* **2010**, *132*, 154104.
[85] S. Grimme, S. Ehrlich, L. Goerigk, *J. Comput. Chem.* **2011**, *32*, 1456.
[86] B. M. Axilrod, E. Teller, *J. Chem. Phys.* **1943**, *11*, 299.
[87] Y. Muto, *J. Phys. Soc. Jpn.* **1943**, *17*, 629.